2004

MAGNETIC RESONANCE IMAGING OF THE HUMAN INFERIOR VENA CAVA DURING LOWER BODY NEGATIVE PRESSURE

Venu Madhav Pothini
University of Kentucky, vmpothini@beckman.com

ABSTRACT OF THESIS

MAGNETIC RESONANCE IMAGING OF THE HUMAN INFERIOR VENA CAVA DURING LOWER BODY NEGATIVE PRESSURE

Magnetic Resonance Imaging (MRI) was used to determine changes in the size of the Inferior Vena Cava (IVC) as a result of blood pooling induced by lower body negative pressure (LBNP). Images of the IVC of supine human subjects (10 males, 10 females) were obtained under four conditions: 1) steady-state 0 mmHg LBNP, 2) steady-state –35 mmHg LBNP, 3) ramping from 0 to –35 mmHg LBNP, 4) ramping from –35 to 0 mmHg LBNP. Volumes for a given IVC segment were obtained under the first two conditions during both end inspiration and end expiration breath-holds. Inferior Vena Cava widths were measured under all four conditions at the levels of portal entry and portal exit. The IVC volume for men and women combined decreased 41% due to LBNP ($p < 1.02 \times 10^{-9}$). The IVC was 64.4% wider at portal exit than at portal entry in men ($p < 0.0003$). Lower Body Negative Pressure induced a decrease in men's vena cava width up to 46% at portal exit and up to 62% at portal entry. Supported by NASA EPSCoR WKU 522611 and NIH GCRC MO1 RR262.

KEYWORDS: Magnetic Resonance (MR), Lower Body Negative Pressure (LBNP), Human Inferior Vena Cava

Author: Venu Madhav Pothini
Date: June 29, 2004

MAGNETIC RESONANCE IMAGING OF THE HUMAN INFERIOR VENA CAVA DURING LOWER BODY NEGATIVE PRESSURE

By

Venu Madhav Pothini

Dr. Charles F. Knapp, Thesis Director

Dr. Abhijit Patwardhan, Director of Graduate Studies

June 29, 2004

RULES FOR THE USE OF THESES

Unpublished theses submitted for the Master's degree and deposited in the University of Kentucky Library are as a rule open for inspection, but are to be used only with due regard to the rights of the authors. Bibliographical references may be noted, but quotations or summaries of parts may be published only with the permission of the author, and with the usual scholarly acknowledgments.

Extensive copying or publication of the thesis in whole or in part also requires the consent of the Dean of Graduate School of the University of Kentucky.

THESIS

Venu Madhav Pothini

The Graduate School

University of Kentucky

2004

MAGNETIC RESONANCE IMAGING OF THE HUMAN INFERIOR VENA CAVA DURING LOWER BODY NEGATIVE PRESSURE

THESIS

A thesis submitted in partial fulfillment of the
requirements for the degree of Master of Science in
The Graduate School
at the University of Kentucky

By

Venu Madhav Pothini

Savage, Minnesota

Director: Dr. Charles F. Knapp, Professor of Biomedical Engineering

Lexington, Kentucky

2004

To my beloved wife Seema G. Pothini for giving me the support, dedication, and extra push to finally finish what I started. I would not have completed this thesis and earned my Master's degree without her.

ACKNOWLEDGMENTS

This thesis was an outcome of research organized and conducted by my advisor, Dr. Charles F. Knapp, and by my mentor, Joyce Evans. Other important participants who prepared experiments, collected data, and monitored subjects included Luna Hilaire, Allison Griffin, Blaine Ott, and Charles Kim of the University of Kentucky Center for Biomedical Engineering, Tammy Ellis and Linda Rice of the University of Kentucky General Clinical Research Center, Dr. Fabio Leonelli from the University of Kentucky Division of Cardiology, and Dr. John Kirsch from the University of Kentucky Magnetic Resonance Imaging and Spectroscopy Center. Image processing software and support were provided by P.L. Charles Fischer of Zedec Technologies, Inc. Thesis review, feedback, and approval were provided by faculty members of the University of Kentucky Center for Biomedical Engineering: Dr. Abhijit Patwardhan, Dr. Peter Hardy, Dr. Betty Sisken, and Dr. Charles F. Knapp. All experiments were part of a NASA EPSCoR (Experimental Program to Stimulate Competitive Research) and NIH GCRC (General Clinical Research Center) study: NASA EPSCoR WKU 522611 and NIH GCRC MO1 RR262.

My parents, Butchamma and Bhaskar Rao Pothini, and my sister, Radhika Pothini, provided support, encouragement, and inspiration to pursue my goal of earning a Master's Degree and to keep it in focus despite my forays into other professional endeavors. My wife, Seema G. Pothini, gave me the focus, discipline, and a much-needed and sustained push to write and complete this thesis.

TABLE OF CONTENTS

LIST OF TABLES

LIST OF FIGURES

LIST OF FILES

VMPthes.pdf (File Size: 818 KB)

1 Introduction

Orthostatic intolerance is a condition characterized by the cardiovascular system's inability to adjust to stresses that impede return of blood to the heart and delivery to the brain. Challenges can be as common as moving from a sitting or supine position to a standing one. Symptoms of orthostatic stress can be as minor as a "head rush" or as problematic as a condition called "syncope." Syncope is characterized by a loss of consciousness resulting from insufficient cerebral perfusion; this end result is a consequence of the cardiovascular system's failure to regulate blood pressure and blood flow [1].

Syncope affects a wide range of people. Astronauts face a significant risk of syncope as a result of prolonged weightlessness [2]. Spinal cord trauma victims often have difficulty regulating against orthostatic stresses during diagnostic and therapeutic procedures that use tilt tables [3]. Many otherwise healthy people also suffer from syncope of unexplained origin.

Given current plans to conduct manned missions to Mars, the risk of syncope in astronauts is of particular interest to NASA and partner space programs. Given current technology, a trip to Mars will take months, exposing astronauts to a weightless environment for a very long time before descending into Mars' gravitational pull [4]. Because prolonged weightlessness has been shown to increase the risk of syncope in astronauts, effective countermeasures are critical to preventing them from succumbing to orthostatic stress far from medical care.

On Earth, six to seven percent of the elderly (60+ years of age) experience syncope annually with 30 percent recurrence within one year of their initial episode. Syncope accounts for three percent of all emergency room visits and up to six percent of general hospital medical admissions, costing roughly $750 million to diagnose and treat. Unexplained syncope, cases in which the root cause of the stress is unknown, accounts for fifty percent of all reported cases [5].

Preventing syncope requires better understanding of the cardiovascular system's responses to orthostatic challenges. Although researchers have conducted research dealing with blood pressure, hormone levels, and fluid flows, information describing volume distributions and shifts within the body has been lacking. Magnetic Resonance

Imaging (MRI) can provide insights to these missing pieces of the puzzle. Applying orthostatic stress within a magnetic bore, however, can be a difficult task because of MRI's limitations including space constraints, MR bore orientation, and exclusion of magnetic materials. Lower Body Negative Pressure (LBNP) is one orthostatic stress that can be used within an MRI system.

Lower Body Negative Pressure causes blood to pool in the lower extremities in a manner similar to the venous pooling that occurs prior to many syncopal episodes. This orthostatic stress has been used to study cardiovascular regulation. Despite the wealth of knowledge that has been accumulated through the use of this technique, few experiments have been conducted to determine fluid volume shifts in specific locations within the vascular system of the human body as a result of exposure to this stress. One important area is the venous side of the circulation because of its high compliance and because of its role in providing venous return during orthostatic stress. The combination of MRI and LBNP provides a unique opportunity to non-invasively identify these changes beyond the capabilities of more global techniques such as impedance measurement and echocardiography.

The objective of the present study was to determine, using MRI, changes in size and shape of the inferior vena cava as a result of the orthostatic stress imposed by LBNP. Measurements were taken during supine control, LBNP-ramping, and steady-state LBNP conditions. The possible relative contributions of biomechanical responses (initial changes during and immediately after ramping LBNP) and regulatory responses (responses during the steady state period following ramping) were also investigated.

2 Background

2.1 Orthostatic Challenge

Orthostatic challenge describes the resistance to blood flow from the lower extremities toward the heart. The cardiovascular system regulates vascular pressure in order to maintain adequate blood flow. As resistance to flow increases, pressure must increase proportionately in order to maintain constant flow.

Equation 1 describes fluid flow as a function of pressure and resistance.

$$\text{Flow} = \text{Pressure} / \text{Resistance} \qquad \text{(Eq. 1)}$$

Fluid pressure can be obtained from Equation 2.

$$P = P_0 + \rho g h \qquad \text{(Eq. 2)}$$

This formula can be applied to the cardiovascular system, where the second component (ρgh) describes the orthostatic challenge (ρ = volume density, g = gravitational acceleration, h = the vertical distance between the lower extremities and the heart).

2.1.1 Orthostatic Stress

Orthostatic stress causes redistribution of fluid within the body. Blood volume shifts within the vasculature because of changes to transmural pressure, causing venous pooling in the lower extremities. This pooling, in turn, reduces mean arterial blood pressure as well as the return of blood flow from the lower body to the heart [6]. These reductions can lead to syncope, depending upon the individual's ability to adapt to the challenge.

2.1.2 Lower Body Negative Pressure

Lower Body Negative Pressure (LBNP) describes the application of vacuum pressure outside the lower body, from the iliac crest of the hip down to the bottom of the feet (see Figure 2.1). Reduction of pressure within the chamber causes a reduction in extravascular pressure, therefore causing an increase in transmural pressure. Although orthostatic stresses induced by tilt and standing do not affect extravascular and transmural pressures in precisely the same way as LBNP, the adaptive mechanisms

triggered by LBNP are consistent with the body's response to other orthostatic challenges [7,8].

LBNP causes a decrease in central blood volume as fluid pools in the lower body, initially collecting in the venous side of the vasculature. As venous structures in the lower body fill, the corresponding increase in hydrostatic pressure draws vascular fluid into the interstitial space [9]. The cardiovascular system therefore loses plasma volume, resulting in lower venous return to the heart. This reduction in central blood volume causes cardiac output and stroke volume to decrease, compromising regulation of arterial blood pressure and blood flow [6]. The cardiovascular system's compensation for these changes includes increases in heart rate and peripheral vascular resistance [10].

Besides being the only method for inducing the pooling of blood within the lower extremities in subjects in a zero gravity environment, LBNP provides a method for creating fluid shifts in a controlled manner on Earth. When considering MR imaging, LBNP provides an optimal orthostatic stress for MRI studies because of physical constraints. A standing or tilt test is not possible with closed, horizontal MR bore units. Thus, LBNP provides a means for applying a consistent, controllable orthostatic stress to subjects within the parameters imposed by the closed, horizontal bore of an MR unit.

These LBNP studies served as a precursor to additional MRI investigations of the effects of six degree head-down bed rest upon the human cardiovascular system [see Figure 2.2]. Six degree head-down tilt provides one accepted tool for studying the effects of prolonged weightlessness on the cardiovascular system. Together, these companion studies provided an extensive view of fluid distribution in the cardiovascular system during control, deconditioning (i.,e, head down bed rest), and application of a provocative stimulus (i.e., LBNP).

2.2 Imaging Technology: Magnetic Resonance

Magnetic Resonance Imaging provided an opportunity to visualize the fluid distribution within the cardiovascular system - as a function of orthostatic stress – with unprecedented resolution and clarity. Some studies have attempted to calculate fluid distribution between whole body segments with impedance plethysmography but are

unable to discriminate between vascular and extravascular space, much less venous and arterial distributions [11, 12]. Some studies utilized ultrasound technology, but lacked the resolution and clarity that MR provides. Magnetic Resonance offers the best combination of measurement accuracy, soft tissue contrast, and resolution compared to other non-invasive techniques for visualizing internal anatomy [13].

2.3 Scanning Planes

MR images are mostly acquired within three fundamental planes: Axial, Coronal, and Sagittal. Figure 2.3 illustrates the Axial and Coronal planes with respect to the MR bore [in which the human body typically lies supine]. The MR bore contains three gradient coils that alter magnetic field strength along each of the principal axes (X, Y, Z). Manipulation of field strength along these axes creates gradients that establish the imaging planes. The magnetic isocenter is the center point of the axes and the center of the bore. Magnetic field strength never changes at this point, even during the application of gradients [14].

2.3.1 Axial

Axial slices are selected by manipulating the Z gradient to alter field strength and precessional frequency along the magnet's Z axis [14]. Axial planes are defined by the X- and Y-axes, as illustrated in Figure 2.3.

2.3.2 Coronal

Coronal slices are selected by manipulating the Y gradient to alter field strength and precessional frequency along the magnet's Y axis [14]. Coronal planes are defined by the X- and Z-axes, as illustrated in Figure 2.3.

2.3.3 Sagittal

Sagittal slices are selected by manipulating the X gradient to alter field strength and precessional frequency along the magnet's X axis [14]. Sagittal planes, not explicitly illustrated in Figure 2.3, are defined by the Y- and Z-axes.

2.3.4 Oblique

Oblique slices are selected by using two gradients in combination [14].

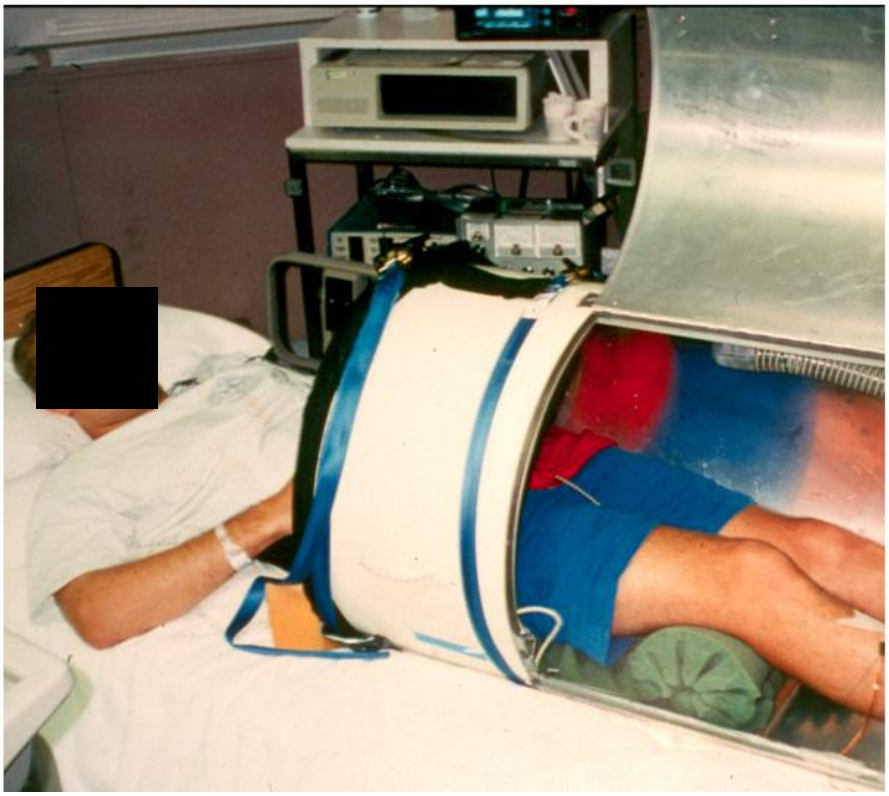

Figure 2.1: Lower Body Negative Pressure Chamber

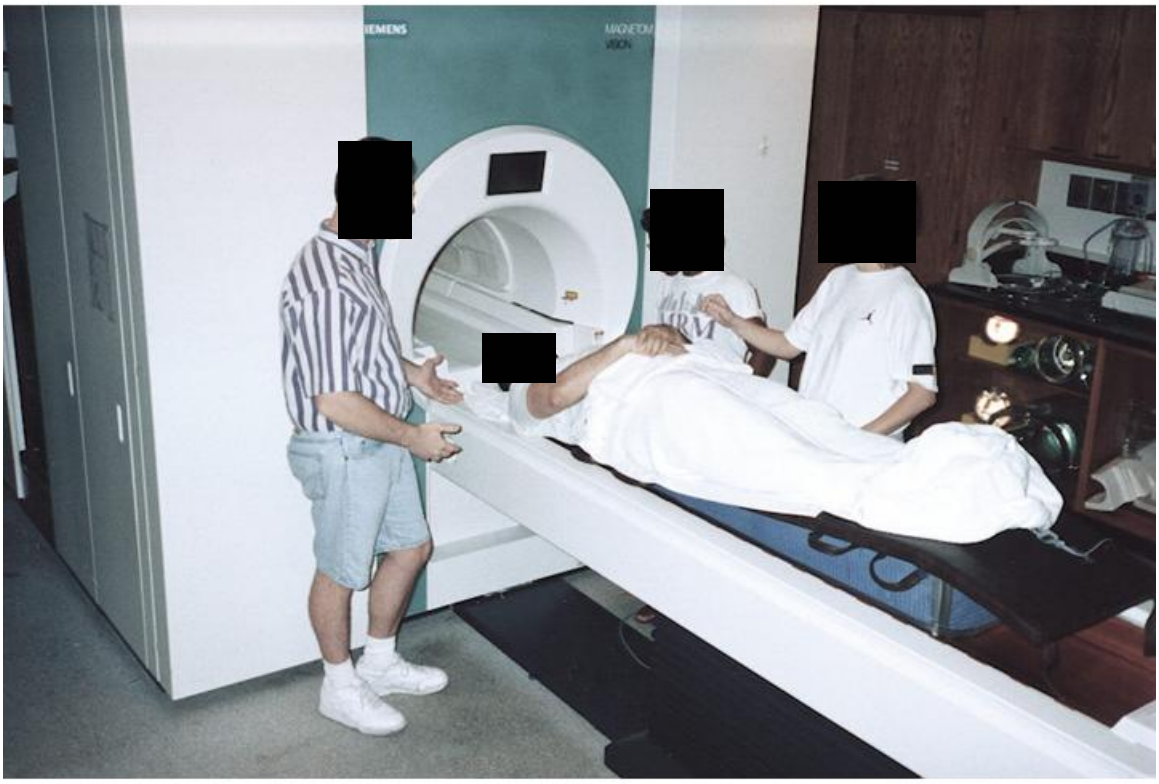

Figure 2.2: Six Degree Head Down Bed Rest Setup in MR Chamber

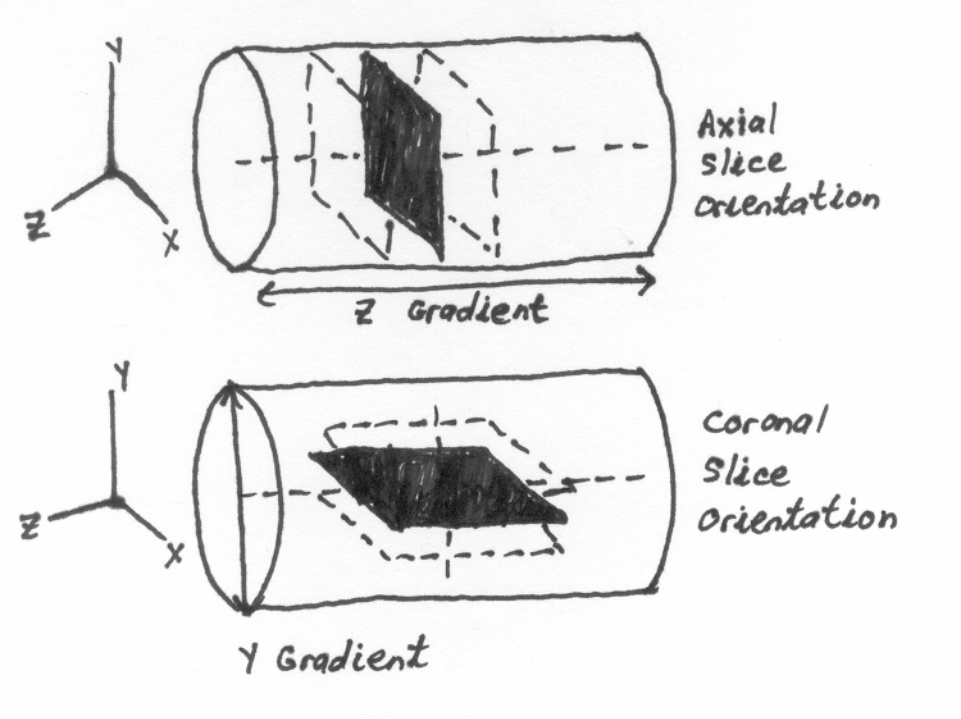

Figure 2.3: Magnetic Resonance Imaging Planes

3 Methods

3.1 Subjects

Data were acquired from studies conducted over a two-year period at the University of Kentucky Clinical Research Center (UK CRC) and at the University of Kentucky Magnetic Resonance Imaging Spectroscopy Center (UK MRISC). The complete subject pool consisted of ten healthy men (178.8 ± 1.8 cm, 77.6 ± 3.4 kg, 25.2 ± 1.0 yr) and ten healthy women (166.8 ± 2.7 cm, 70.9 ± 2.9 kg, 25.8 ± 1.2 yr). All women's menstrual periods were naturally cycling. They were studied between days two and ten of their menstrual cycle. Men were studied in the first year during a three-month period, and women were studied during a three-month period in the second year.

All volunteers were oriented to LBNP and to the MRI chamber at least one week prior to participation in the study. Orientation also included screening for habits (e.g., smoking) and medical conditions (e.g., cardiovascular disease) that would have disqualified them from participation. All subjects provided written consent to the test protocols approved by the local Institutional Review Board (IRB approval 91-00012).

3.2 Study Protocol

Table 3.1 outlines the experimental protocol used with each volunteer. Note that with alternating subjects, the MRI studies preceded the CRC studies.

3.3 MR Imaging Setup

3.3.1 MRI Chamber

The MRI system was a 1.5 Tesla Siemens system. The MR bore was 60 centimeters in diameter, making it wide enough to accommodate an LBNP chamber. The bore of the MR imager was easily long enough to contain an LBNP chamber since the MR bore was designed to fit human adults from head to toe.

3.3.2 LBNP Chamber

The Lower Body Negative Pressure (LBNP) Chamber used in the MR imaging experiments was specially constructed from nonmagnetic materials such as different forms of plastic. Because of the magnet's strength, even small magnetic objects can become lethal projectiles; magnetic materials in the LBNP chamber could have also produced image artifacts. These risks motivated the construction of the LBNP chamber with nonmagnetic materials. The chamber's size was also restricted to fit within the MRI chamber. Consequently, the LBNP chamber used in the MRISC was 48 centimeters [19 inches] in diameter and 125.5 centimeters [50 inches] long. By contrast, the standard LBNP chamber that was used in the CRC was 52.71 centimeters [21 inches in diameter] and 120.48 centimeters [48 inches long].

3.4 Imaging Sequences

3.4.1 Time Of Flight

Magnetic Resonance signals are sensitive to flow and to motion [15]. Hydrogen nuclei that move during image acquisition can create flow motion artifacts such as "phase ghosting" or "time of flight" displacement [14].

In order to produce a spin echo MR signal, a nucleus must receive both an excitation pulse and a rephasing pulse. In a spin echo sequence, if a nucleus only receives one of these two pulses, it does not produce an spin echo and hence no MR signal is received. Stationary nuclei within the region of the excitation coil always receive both pulses, but moving nuclei might only receive the excitation pulse before moving through the targeted slice, thereby missing the rephasing pulse. Other moving nuclei might lie outside the imaging plane during the excitation pulse but then enter the imaging plane in time to receive the rephasing pulse. This condition in which nuclei receive one of the two pulses describes time of flight [14].

The inflow and outflow of spins in a spin echo sequence result in variations in the amplitude of the signal due to the different history of RF pulses each spin receives during its transit of the image slice. This effect is due strictly to the RF pulses and exists even in the absence of imaging gradients. In addition to this effect, the amplitude of the

total signal is affected by the presence of imaging gradients. To reduce the dependence of the signal on the velocity of motion, imaging sequences incorporate techniques known as gradient moment nulling and gradient moment rephasing. Additionally, by making the initial inversion pulse non-spatially selective (exciting the entire imaging region rather than a specific part of the imaging region such as the inferior vena cava), the effects of multiple pulses on the image wind up being relatively inconsequential.

One method of compensating for the effects of flowing nuclei on image quality, particularly in the case of venous blood flow, is the application of "gradient moment rephasing" which compensates for the altered phase values of nuclei flowing along a gradient. By using additional gradients to force the altered phases back to their original values, the flowing nuclei do not change phase when exposed to the main gradient [14]. Because these flowing nuclei have the same phase as stationary nuclei, their signals combine to create an even more intense, brighter signal within the slice [14]. Increased signal from fresh, previously unexcited nuclei flowing into the imaged region is known as "Inflow Signal Enhancement" [15].

The Time of Flight imaging sequences of this study utilized gradient moment rephasing to establish gray levels that were dependent upon Inflow Signal Enhancement. Because of the cumulative effect of flowing nuclei, the highest velocity appeared as white and zero velocity appeared as black. This technique was very useful for imaging vascular structures with laminar flow such as the inferior vena cava. Because image gray level correlated to velocity profile, the shape of the inferior vena cava itself could be captured due to the velocity profile of blood through that structure. Additionally, the initial inversion pulse was non-spatially selective, diminishing the effects of the multiple pulses on image clarity.

In structures with laminar flow such as the inferior vena cava, fluid velocity is generally highest in the center and approaches zero at the vessel walls. Velocity profiles may be parabolic or more blunt in shape, depending upon flow conditions. A time of flight image of this vessel would appear brightest in the center and decrease in image brightness toward the vessel walls which would appear black, providing clear definition of the interior walls of the vessels, as illustrated in figure 3.3.

Although time of flight imaging can provide a very powerful tool for capturing the walls of venous structures, it does have limitations. Subject motion during a time of flight scan can cause misregistration of the image. Pulsatile flow of blood can also cause motion artifacts including blurring, making arterial structures such as the aorta more difficult to accurately capture [16].

3.4.2 Breath Holds

Acquisition of images during breath holds reduces breathing-related artifacts such as ghosting, blurring, and misregistration [17]. Misregistration can still occur if the flow is oblique within the image plane. It arises from the difference in time between the phase encoding and the frequency encoding gradients. The purpose of capturing images during breath holds was to isolate the contributions of respiration from the effects of LBNP on changes in vena cava dimensions. Images during end-inspiration and end-expiration were captured during steady-state –35 mmHg LBNP and during 0 mmHg control.

3.4.3 TurboFLASH

TurboFLASH is a fast image acquisition technique that captures each image in less than two seconds. Coupled with echogating (timing image acquisition to heart beat), this acquisition eliminates motion artifacts related to heart motion and lower frequency cycles such as breathing. The reduced image resolution of this acquisition reduces edge definition, making it harder to identify vessel walls [14]. Despite its imprecision for edge detection, the speed of image acquisition made TurboFLASH a desirable technique for visualizing changes to the size and shape of the inferior vena cava as LBNP was ramped during the relatively brief span of one minute. Figure 3.4 illustrates an example of a TurboFLASH image of the inferior vena cava as it passes through the liver.

3.5 Data Processing

Images were analyzed with QuantIm image processing software by Zedec Technologies, Inc. The raw images were transferred from the Siemens MRI system to a UNIX-based workstation that had been loaded with the software. After loading an axial

or coronal image of the vena cava into the software package, the vena cava was separated from the rest of the image by using a variety of techniques.

For example, in several time of flight images, venous branches that led into the vena cava had to be distinguished from the vena cava, requiring manual separation (segmentation) within the images. Some time of flight images were affected by pulsatile blood flow in the aorta which caused the image of the aorta to smear, sometimes into the image of the vena cava; manual separation of the imaged vessels was necessary in these cases, too.

Separation of the vena cava from the rest of the image was facilitated by manually drawing a boundary along the vessel edge. The software's "Segment" function then used gray levels to identify discrete structures. Utilization of a Sobel filter enhanced the precision of vessel identification. The Sobel filter improved the accuracy of edge detection by focusing on sharp changes and ignoring noise. The Sobel filter, the sum of two convolutions, applied the algorithm in Equation 3.

$$G_0(x,y) = |D_{xi}(x,y)| + |D_{yi}(x,y)| \quad \text{(Eq. 3)}$$

D_{xi} was the gradient of the image in x, and D_{yi} was the gradient of the image in y [18].

Following user selection of the isolated vena cava, the software created an image contour map, selecting the outermost, continuous path of pixels corresponding to the vessel edge. The contour map defined a Cartesian coordinate pair for each pixel. The Cartesian coordinate pairs were then used to measure cross sectional area, perimeter, maximum diameter, minimum diameter, angle of maximum diameter, and angle of minimum diameter.

Gray scale mapping was only used with the coronal images and with the purpose of enhancing the precision of vessel identification. It required the user to draw a "profile line" across a region of interest. The software then plotted gray levels of the image across the user-defined lined, as depicted in Figure 3.5. The output of this function provided valuable information to the user for accurately and precisely defining the vessel edges.

In order to compare volumes that were imaged before and during steady-state LBNP, the imaged regions had to be matched. Axial vena cava images were matched by consistently targeting the region beginning at the tenth thoracic vertebra. Matching

was also confirmed following image acquisition but prior to data processing by examining photographic films containing every slice in each data series. By mounting this film onto a light box, multiple data sets could be compared side-by-side to confirm the presence of specific landmarks. Axial slices of the vena cava were matched by a fixed, rigid coordinate system that was based on the tenth thoracic vertebra. Although we always imaged a 3.6 cm length of the inferior vena cava beginning at the level of the tenth thoracic vertebra and progressing toward the level of the eleventh thoracic vertebra, we cannot guarantee that the 3.6 cm vena cava segment that was measured during control was the exact same 3.6 cm segment that was measured during –35 mmHg LBNP. The inferior vena cava could have shifted along the Z-axis as a result of LBNP, causing us to image a different segment of the inferior vena cava.

In an attempt to ensure analysis of the same inferior vena cava segment under all conditions, coronal vena cava images were obtained from the same plane in fixed space. This plane was selected by comparing several adjacent coronal images of the liver, seeking a slice that clearly showed the inferior vena cava traversing the liver from portal entry to portal exit. Figure 3.7 shows four adjacent coronal slices across the liver. Slice B is the only one of these slices that includes a clear image of the inferior vena cava as it traverses the liver from portal entry to portal exit. The physical space corresponding to this slice was then selected for obtaining eighteen coronal TurboFLASH images as LBNP was ramped from 0 to –35 mmHg ("LBNP ramp-up") or from –35 to 0 mmHg ("LBNP ramp-down"). This physical space was also imaged six times during the first minute of steady-state control and steady-state –35 mmHg LBNP. Because each subject went through two LBNP applications in the MR chamber, two sets of these data were available for each subject. Review of the images, however, provided two complete sets for five male subjects but no complete sets for the female subjects. For several female subjects, the inferior vena cava was not captured at all during LBNP ramp-up. For the remaining female subjects, the inferior vena cava disappeared from the images before completion of LBNP ramp-up. In the complete sets, the vena cava was visible throughout each ramping process and during the first minute of each steady-state condition (0 mmHg and –35 mmHg).

Table 3.1: Experimental Protocol

Time	Step
7:00 PM	Admit subject to UK CRC. Fluid I/O begins. Record subject height, weight, age, and calf circumference.
9:00 PM	Research staff leave floor nurses to begin monitoring subject activity.
10:00 PM	Check blood pressure, heart rate, and offer snacks.
7:00 AM	Awaken subject. Apply intravenous (antecubital) catheter with heplock to subject's right arm. Walk around hospital.
7:30 AM	Subject eats a light, low fat, low protein breakfast.
8:00 AM	Subject lies in supine position. Apply sensors for arterial pressure, thoracic impedance, ECG, Calf Circumference, radial artery flow, and skin flows.
8:30 AM	Begin recording 20 minutes of control data (subject is supine and resting).
8:45 AM	Draw 0.5 cc hematocrit blood samples in one-minute intervals for four minutes (2 cc).
8:49 AM	Draw hormonal blood samples (9 cc).
8:50 AM	End control and begin LBNP/LBPP (15 minutes each with an intervening five minute break) protocols (randomized by subject). Draw hormonal blood samples during the final two minutes of LBNP (-35 mmHg) and during the final two minutes of LBPP (+15 mmHg). Continue drawing 0.5 cc hematocrit blood samples during LBNP and during the first five minutes of recovery following LBNP. (13.5 cc) Continue drawing 0.5 cc hematocrit blood samples during LBPP and during the first five minutes of recovery following LBPP (13.5 + 2cc control).
9:40 AM	Complete first run. Set up for echocardiogram studies.
10:00 AM	Begin recording ten minutes of echocardiography control data (e.g, End Diastolic Volume, End Stroke Volume).
10:10 AM	Begin fifteen minutes of LBNP.

(continued on next page)

Table 3.1: Experimental Protocol (continued from previous page)

Time	Step
10:25 AM	End LBNP and begin five minutes of recovery.
10:30 AM	Subject ambulatory for light snack and transport to MRISC.
11:00 AM	Subject lies in supine position on MRI table.
11:05 AM	Apply sensors for LBNP, ECG, Arterial Pressure, temperature, PO_2, and CO_2.
11:20 AM	Acquire MRI anatomical images while repeating resting control, LBNP and LBPP protocols [without blood draws].
12:00 PM	Change MRI parameters for perfusion and diffusion data collection.
12:20 AM	Acquire MRI perfusion and diffusion images while repeating resting control, LBNP and LBPP protocols [without blood draws].
1:00 PM	Subject ambulatory for lunch.
1:15 PM	Check fluid balance and remove venous catheter.
1:30 PM	Dismiss subject.

Figure 3.1: (left) LBNP Chamber in MR Imager, View from Back of Magnet; (right) LBNP Chamber and Experimental Subject in MR Imager, View from Front of Magnet

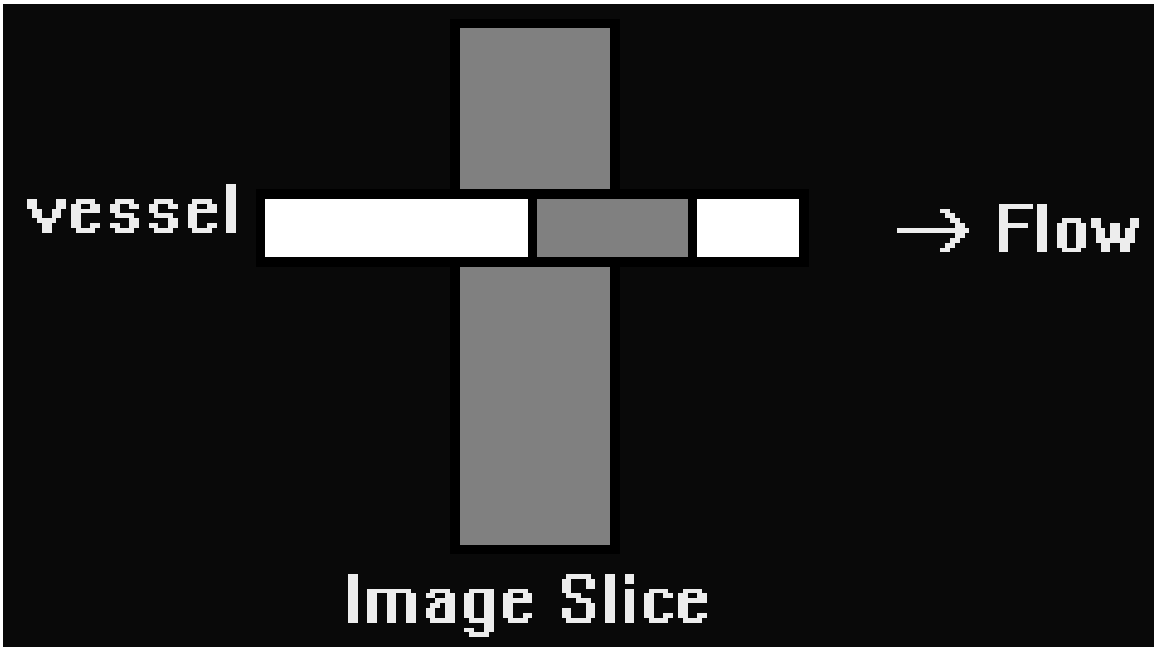

Figure 3.2: Time of Flight Conceptual Drawing

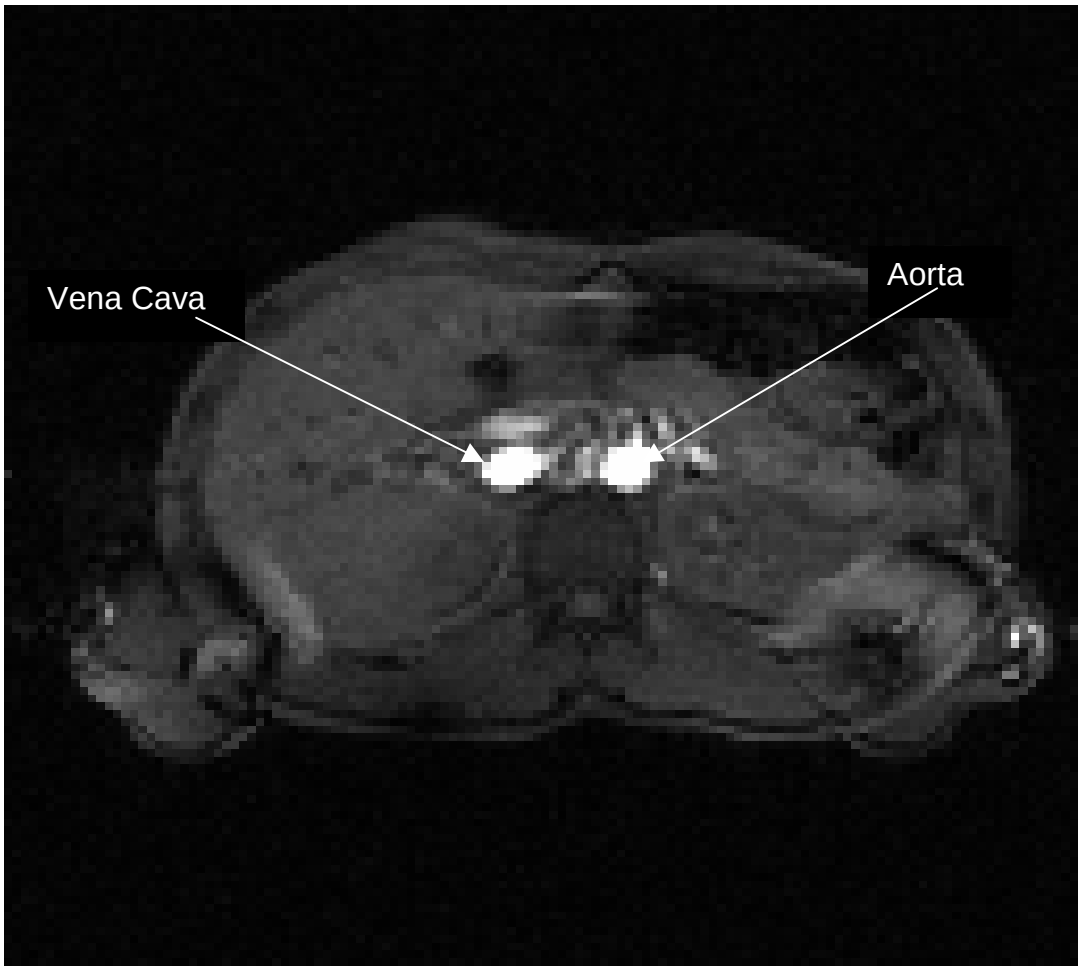

Figure 3.3: Example of Time of Flight Image of Inferior Vena Cava

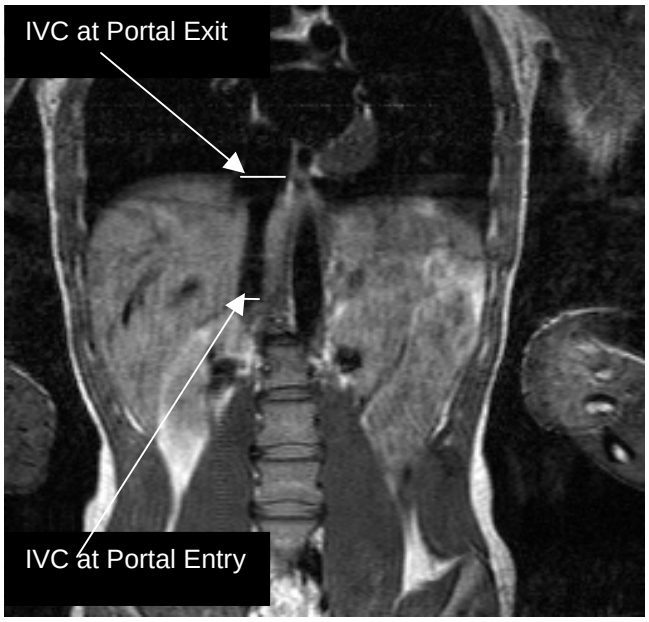

Figure 3.4: Example of TurboFLASH Image of Inferior Vena Cava

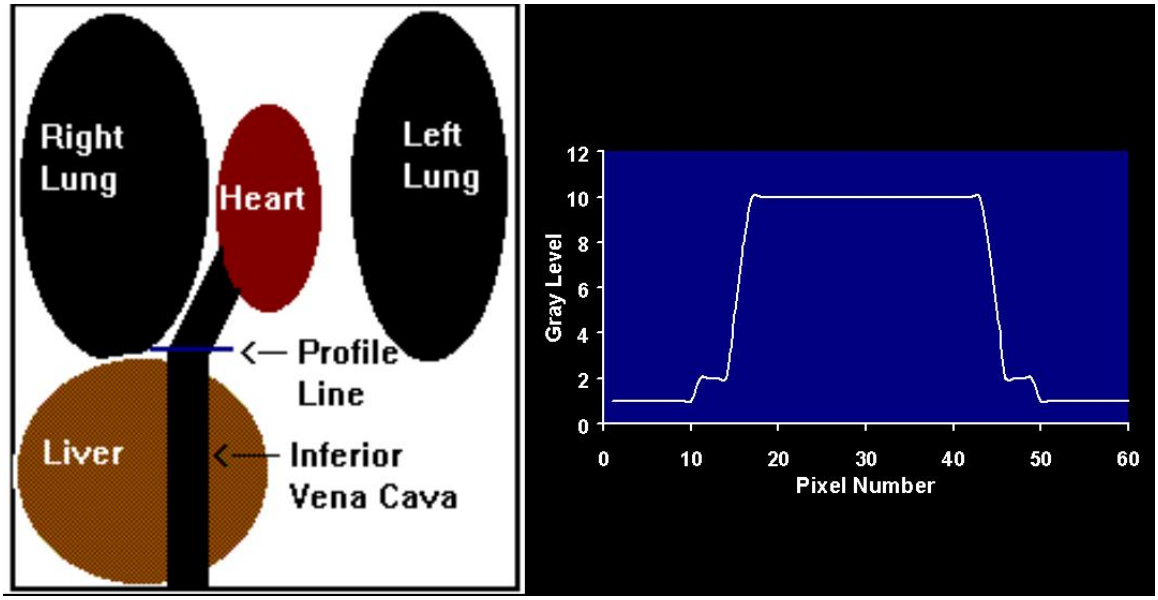

Figure 3.5: Gray Scale Mapping of the Inferior Vena Cava and Adjacent Tissue

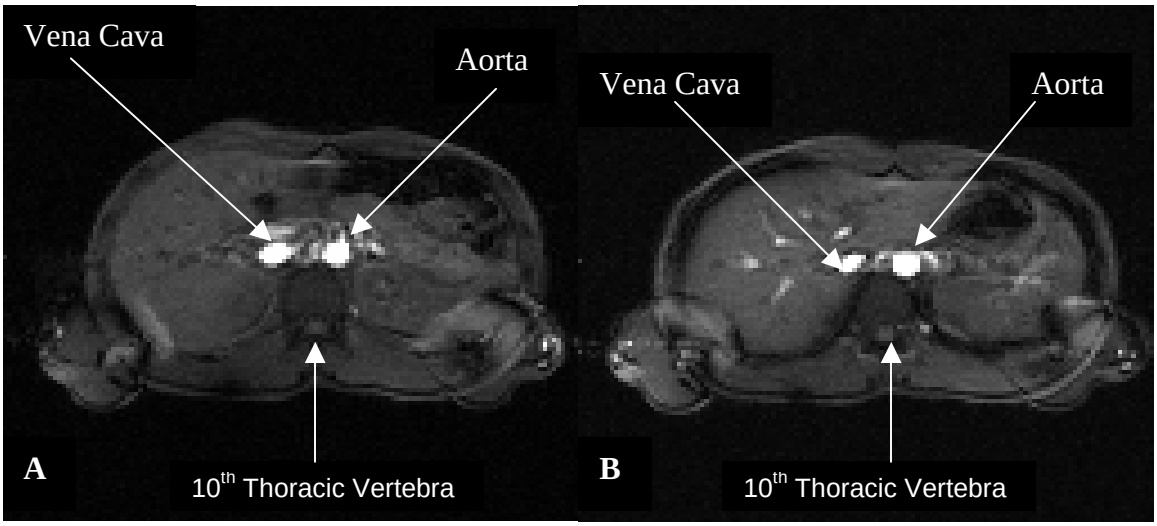

Figure 3.6: Example of Matched Axial Vena Cava Images – A) Pre-LBNP, B) –35 mmHg LBNP

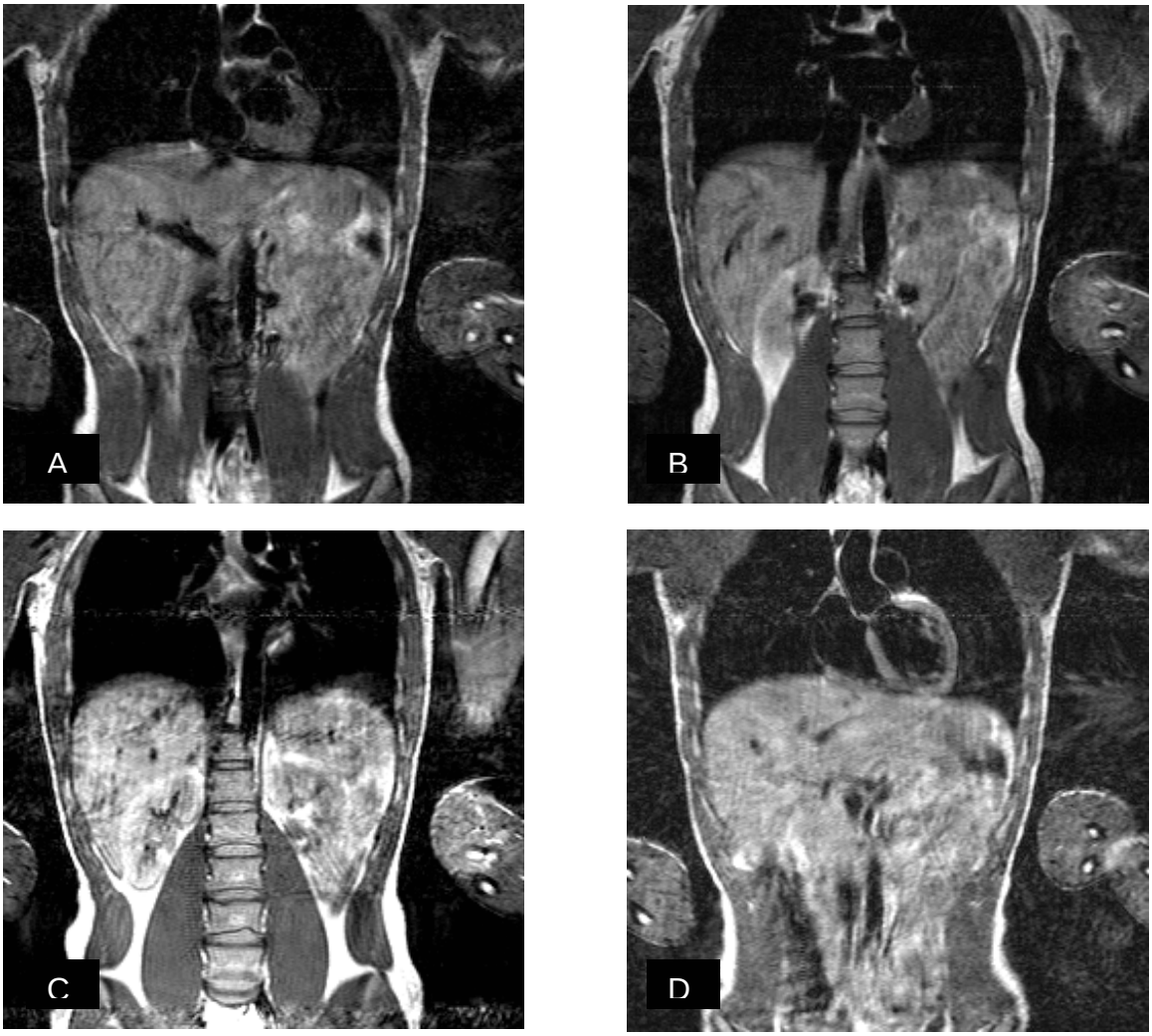

Figure 3.7: Coronal, T1 Weighted Slices Across Liver Obtained to Identify the Inferior Vena Cava

4 Results

4.1 Cross-sectional Area of Inferior Vena Cava

For each subject, a 3.6 centimeter length of the Inferior Vena Cava (IVC) starting at the level of the tenth thoracic vertebra and proceeding toward the level of the eleventh thoracic vertebra was imaged as six consecutive, adjacent, non-overlapping 0.6 centimeter axial slices. This region was measured during steady state pre-LBNP [0 mmHg] and during steady state LBNP [–35 mmHg]. During each steady state condition, the region was imaged twice: once during end inspiration breath hold and once during end expiration breath hold. The Time-Of-Flight imaging sequence was utilized to acquire these images. Assuming uniform cross-sectional area of the IVC within each slice, volume of the imaged region of the vessel was calculated by Equation 4.

$$\text{Volume} = 0.6 \sum \text{Area}_i \qquad \text{(Eq. 4)}$$

Four factor Analysis of Variance of the data identified which variables and interactions were significant. The four factors in the model were

1) Gender [male versus female],
2) LBNP [0 mmHg versus –35 mmHg],
3) Breath Hold [end inspiration versus end expiration], and
4) Subject ID [1 through 20].

Gender ($p < 0.0005$), LBNP ($p < 1.02211 \times 10^{-9}$), and Subject ID ($p < 3.30052 \times 10^{-9}$) were significant main factors. Breath Hold ($p < 0.395282$) was not a significant main factor. Although Gender and LBNP were individually significant, their interaction was not statistically significant ($p < 0.695876$).

Although gender was a significant factor with the non-normalized data, it was no longer significant after normalization against body surface area ($p < 0.19$). Body surface area was calculated by using the Mosteller Formula shown in Equation 5.

$$\text{Body Surface Area } (m^2) = ([\text{Height(cm)} \times \text{Weight(kg)}]/3600)^{1/2} \qquad \text{(Eq. 5)}$$

Figure 4.1illustrates the volume of the selected section of the IVC as a function of gender, LBNP, and respiration. This graphical presentation of the data visually reinforces the statistical conclusions. Comparisons between end inspiration and end expiration breath holds do not suggest any clear relationship between respiration and

volume of the inferior vena cava at the level of the tenth thoracic vertebra. At 0 mmHg, IVC volume was two percent smaller during end inspiration than during end expiration; at –35 mmHg, IVC volume was 22% larger during end inspiration than during end expiration. However, these differences were not statistically significant ($p < 0.395$). Because respiration was not a statistically significant factor, and because the interaction between respiration and LBNP was not statistically significant, the 22% difference in IVC volume between breath holds during –35 mmHg LBNP could not, for the purposes of this study, be used to represent a change that can be directly attributed to either respiration, LBNP, or their interaction.

Although differences due to breathing were not statistically significant, the differences due to gender and LBNP were. The breath hold data in Figure 4.1 were regrouped in order to generate the data in Figure 4.2. For each combination of gender and LBNP (e.g., women at 0 mmHg, women at –35 mmHg, men at 0 mmHg, men at –35 mmHg), the end expiration and end inspiration breath hold data were combined. Figure 4.2 illustrates the volume of the selected section of the inferior vena cava as a function of gender and LBNP but independent of respiration. During control conditions (0 mmHg), women's IVC volume was 17% smaller than men's IVC volume. During steady-state –35 mmHg LBNP, women's IVC volume was 32% smaller than men's IVC volume. Men's IVC volume decreased 36% from control to –35 mmHg LBNP; women's inferior vena cava volume decreased 48% from control to –35 mmHg.

4.2 Time History Changes in the Width of the Inferior Vena Cava

In order to observe the immediate impact of LBNP on the inferior vena cava, eighteen coronal images of the IVC, where the IVC traversed the liver, were acquired over the minute that pressure was steadily ramped from 0 to –35 mmHg ("LBNP ramp-up"). Six more coronal images of the same IVC section were imaged during the first minute of steady state LBNP. Similarly, eighteen coronal images of the IVC were acquired over the minute that pressure was steadily ramped from -35 to 0 mmHg ("LBNP ramp-down"); and six more images were acquired during the first minute of steady state recovery. The TurboFLASH imaging sequence was utilized to acquire these images. The width of the IVC was measured both where it entered the liver

("portal entry") and where it exited the liver ("portal exit"). The descriptions "portal entry" and "portal exit" have been assigned with respect to the direction of blood flow in the inferior vena cava through the liver, toward the heart. The resulting data is illustrated in Figure 4.3.

During control and recovery, vena cava width at portal exit (VCW_{exit}) was 64.4% larger than vena cava width at portal entry ($VCW_{entrance}$) ($p < 0.0003$). As Figure 4.3 clearly illustrates, VCW_{exit} was always larger than $VCW_{entrance}$. LBNP ramp-up caused VCW to decrease at both measurement sites ($p < 0.001$). From control to the end of LBNP ramp-up, $VCW_{entrance}$ decreased by 61.6% and VCW_{exit} decreased by 45.8%.

During the first minute of steady-state –35 mmHg LBNP, both $VCW_{entrance}$ and VCW_{exit} exhibited a "rebound" effect by increasing 13% and 21.2% of their original control values, respectively. This moderate recovery was statistically significant ($p < 0.005$). Interestingly, neither measurement site appeared to continue recovering past the first minute of steady-state –35 mmHg LBNP; this observation is based on the negligible difference between each measurement site's width one minute into steady-state –35 mmHg LBNP and fourteen minutes into steady-state –35 mmHg LBNP. During LBNP ramp-down, both $VCW_{entrance}$ and VCW_{exit} completed recovery toward their initial control values.

The decreases in VCW at both measurement sites during LBNP ramp-up appear to be quadratic functions of time or LBNP (assuming the rate of change of LBNP was constant). Figure 4.4 focuses on the LBNP ramp-up portion of the VCW data set. The following relationships were obtained:

For $VCW_{entrance}$ as a function of LBNP during ramp-up:

$$VCW_{entrance} = 0.0096(LBNP)^2+0.6731(LBNP)+20.096,\ R^2 = 0.9654 \qquad \text{(Eq. 6)}$$

For VCW_{exit} as a function of LBNP during ramp-up:

$$VCW_{exit} = 0.114(LBNP)^2+0.7869(LBNP)+31.13,\ R^2 = 0.9629 \qquad \text{(Eq. 7)}$$

Vena Cava Width changes at both measurement sites during the first minute of steady-state LBNP appear to be linear functions of time [but not of LBNP since it was held constant]. Figure 4.5 illustrates the steady-state –35 mmHg LBNP portion of the VCW data set. The following relationships were obtained:

For $VCW_{entrance}$ as a function of time during steady-state LBNP:

$VCW_{entrance}$ = 0.0592(time)+8.7172, R^2 = 0.995 (Eq. 8)

For VCW_{exit} as a function of time during steady-state LBNP:

VCW_{exit} = 0.0503(time)+18.117, R^2 = 0.9712 (Eq. 9).

Vena Cava Width changes at both measurement sites during LBNP ramp-down appear to be linear functions of time or LBNP. Figure 4.6 focuses on the LBNP ramp-down portion of the VCW data set. The following relationships were obtained:

For $VCW_{entrance}$ as a function of LBNP during ramp-down:

$VCW_{entrance}$ = 0.224(LBNP)+20.255, R^2 = 0.9892 (Eq. 10)

For VCW_{exit} as a function of LBNP during ramp-down:

VCW_{exit} = 0.2534(LBNP)+32.244, R^2 = 0.9645 (Eq. 11)

The high R^2 values for Equations 6 through 11 suggest that each equation provides a very good fit against the available data.

Vena Cava Width changes at both measurement sites during the first minute of recovery do not appear to fit a linear or quadratic equation. Changes during this period appear to be a combination of return to original control values along with some variation due to noise. Figure 4.7 shows the recovery portion of the VCW data set. The R^2 values corresponding to the equations for recovery are not as high as the R^2 values corresponding to the other equations mentioned above, making the recovery equations tenuous approximations.

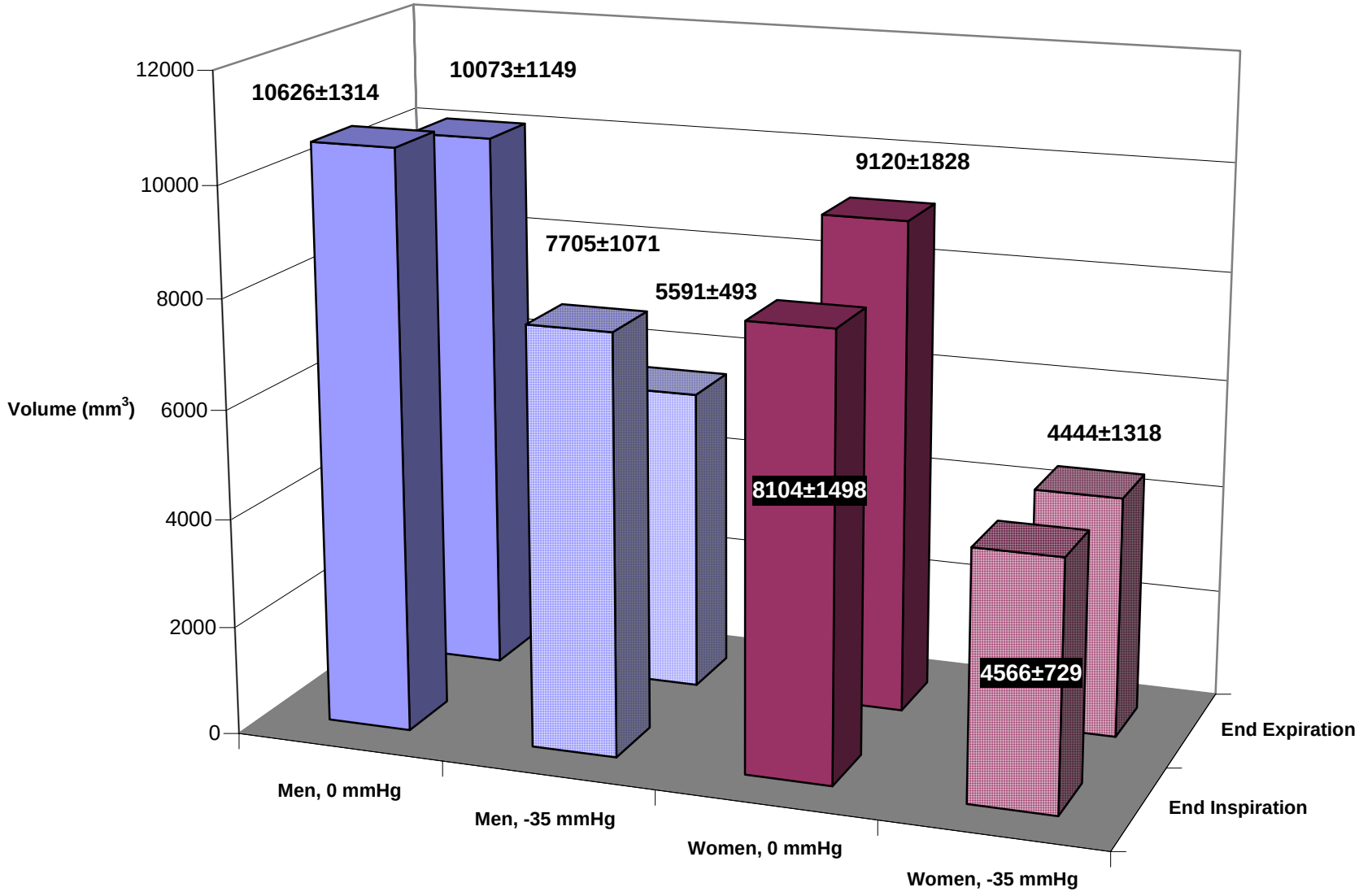

Figure 4.1: Inferior Vena Cava Volume vs. Gender, LBNP, Respiration

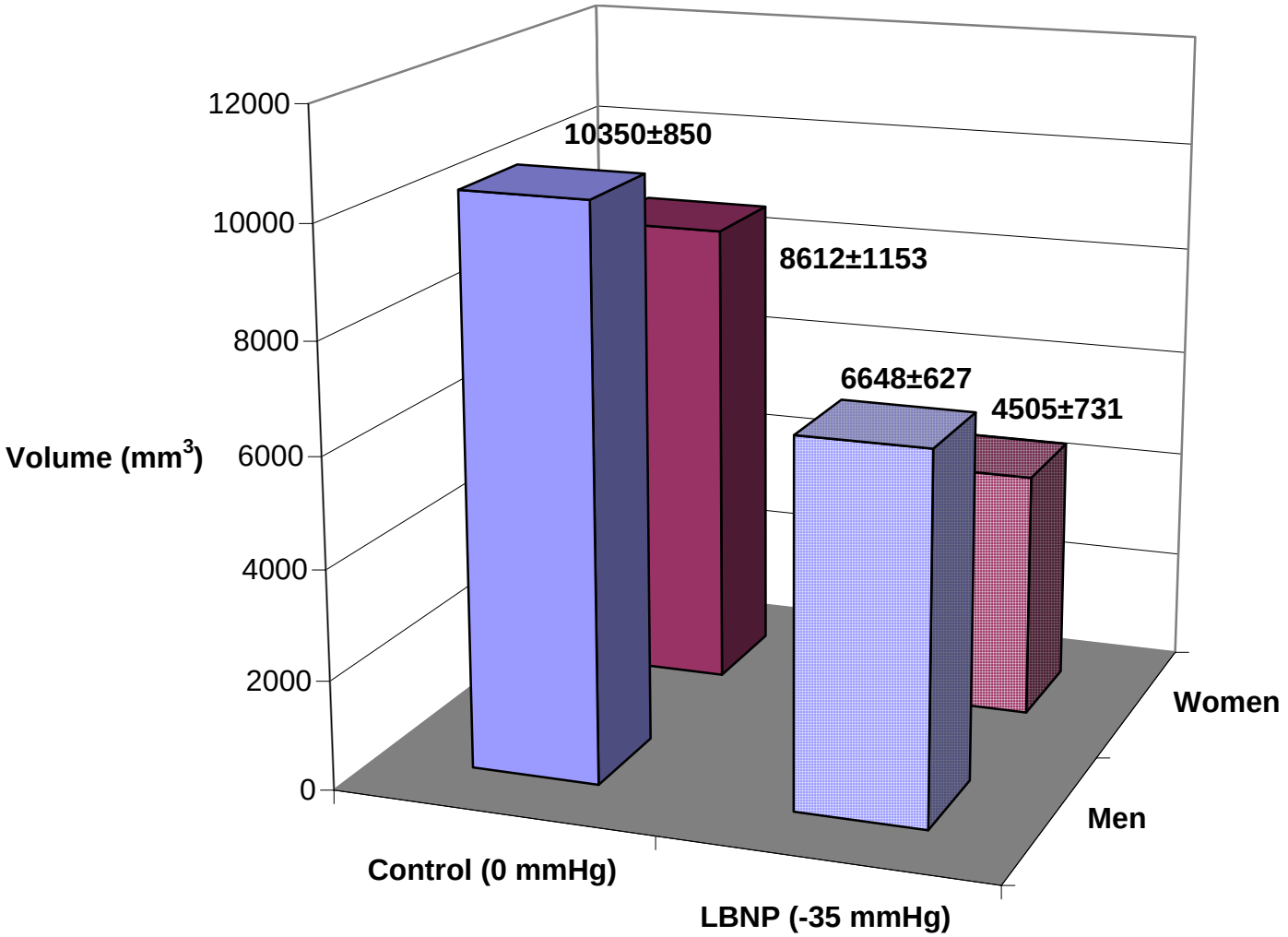

Figure 4.2: Inferior Vena Cava Volume vs. Gender, Lower Body Negative Pressure

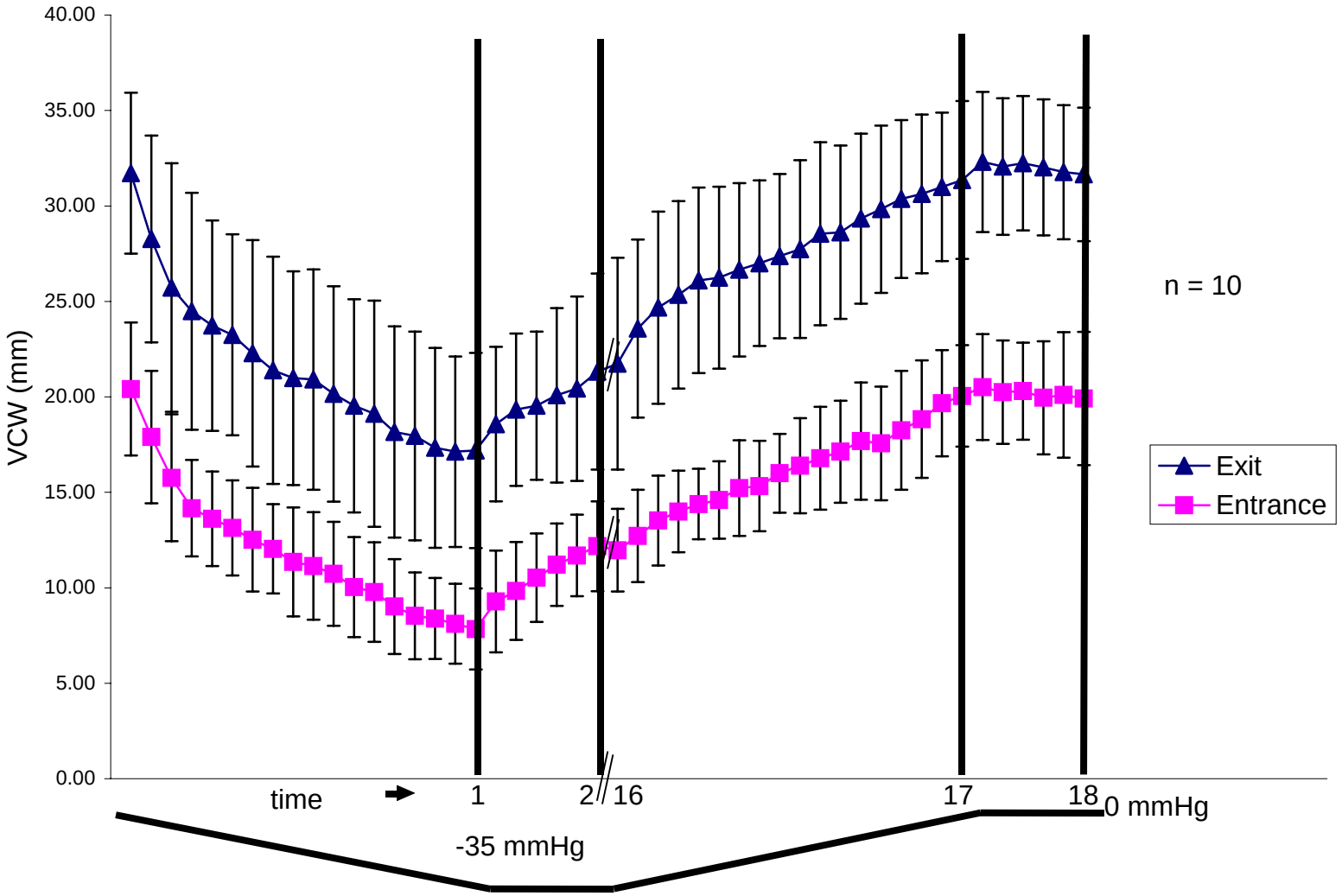

Figure 4.3: Vena Cava Width versus Lower Body Negative Pressure

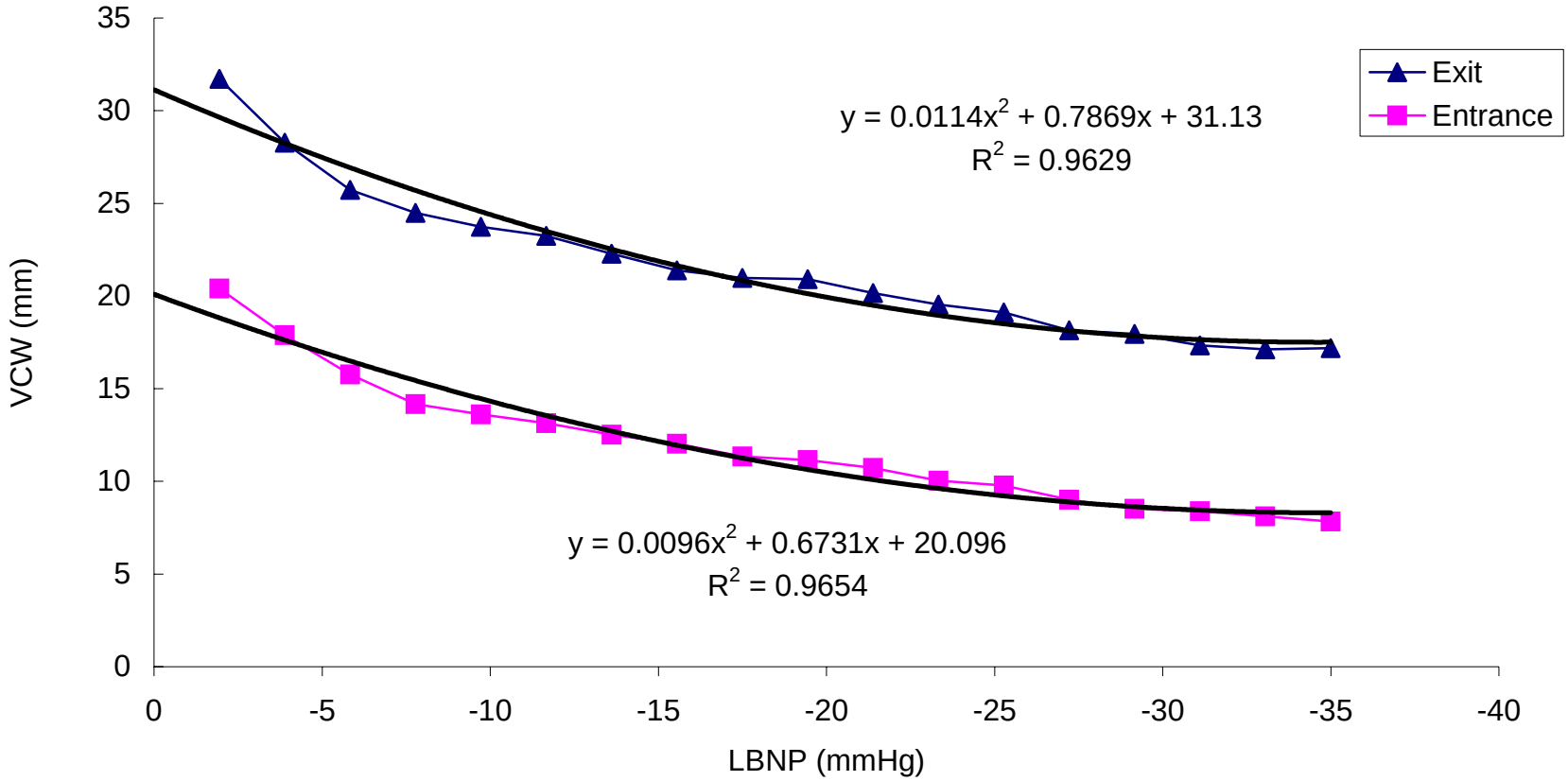

Figure 4.4: Vena Cava Width during Lower Body Negative Pressure Ramp-Up

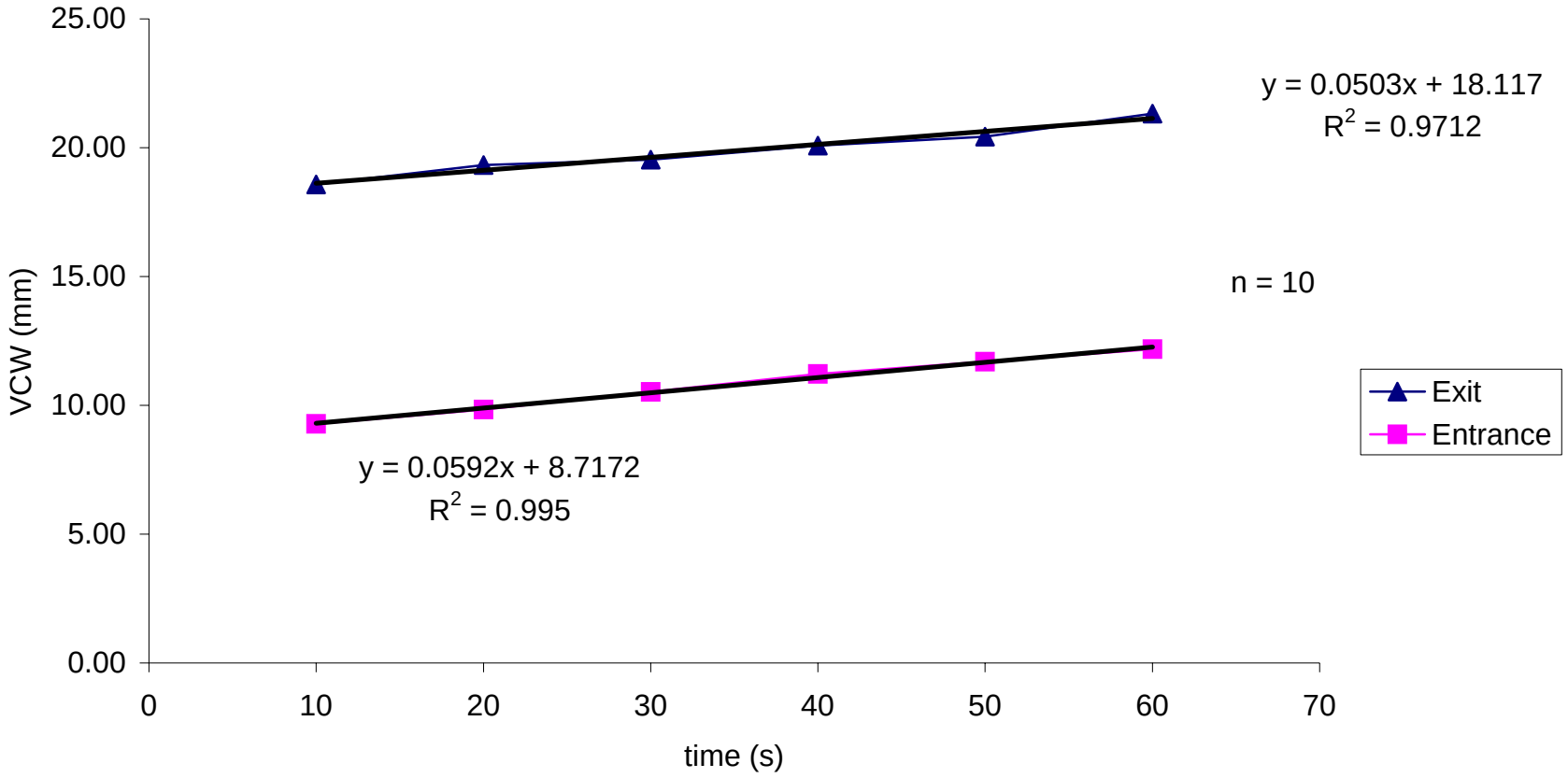

Figure 4.5: Vena Cava Width During First Minute Steady-State Lower Body Negative Pressure

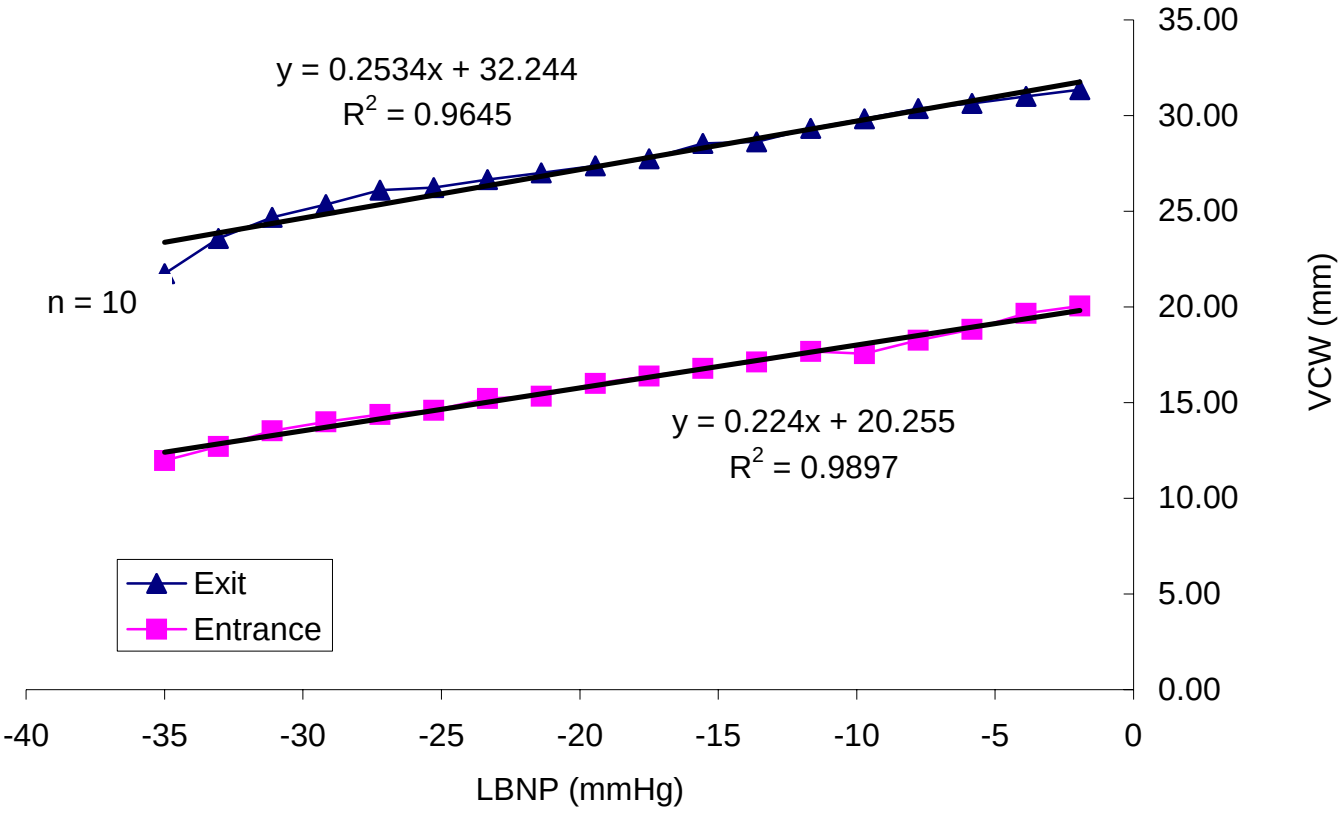

Figure 4.6: Vena Cava Width During Lower Body Negative Pressure Ramp-Down

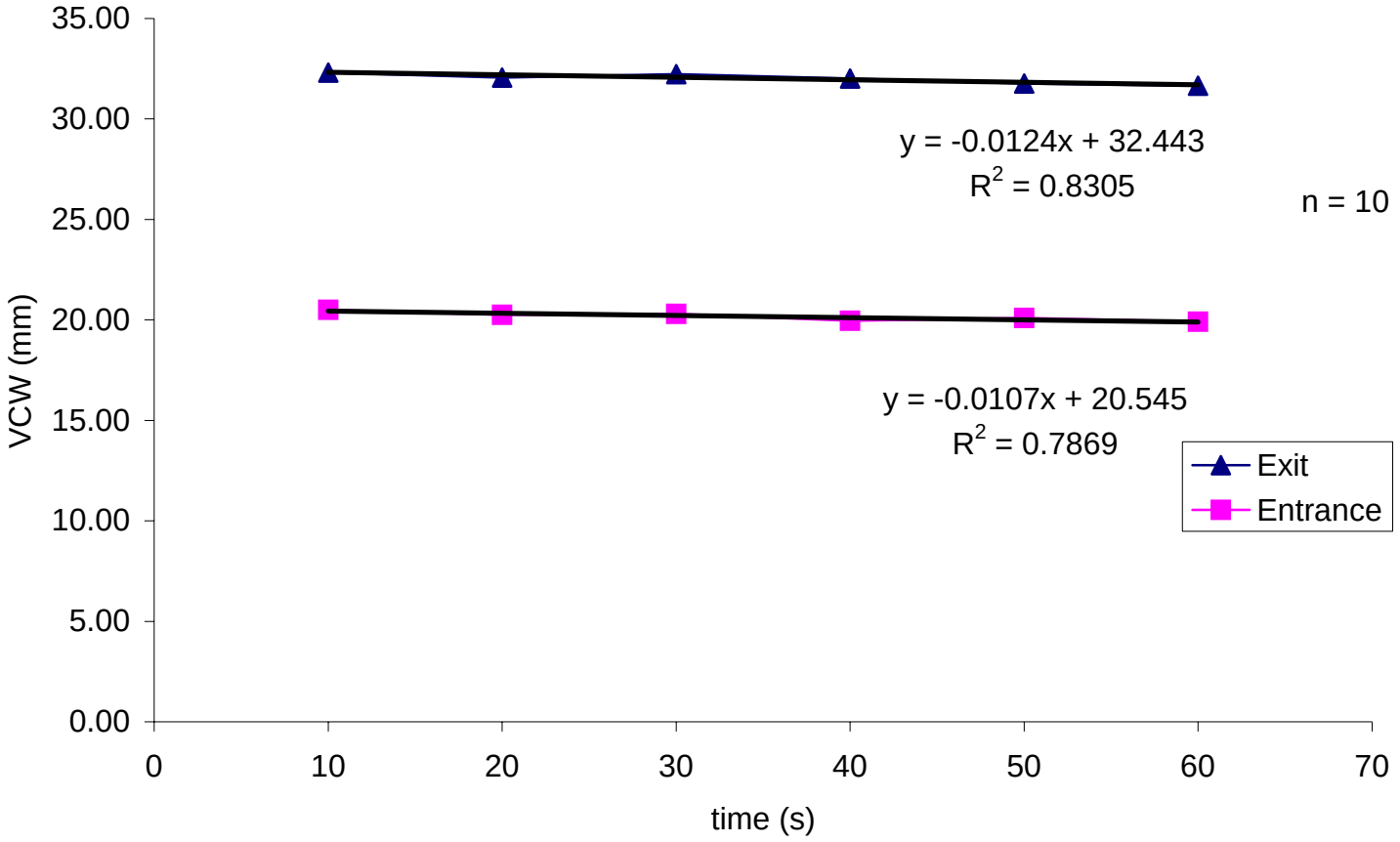

Figure 4.7: Vena Cava Width During First Minute Steady-State Recovery

5 Discussion

5.1 Volume of the Abdominal Inferior Vena Cava

In the present study, the lack of a statistically significant relationship between breath holds and volume of the inferior vena cava at the entrance and exit of the liver appears to be inconsistent with existing knowledge of relationships between respiration and volume of the inferior vena cava. An ultrasound study of 85 humans subjects observed partial collapse of the inferior vena cava during inspiration and maximum distension at end expiration [19]. A subsequent study of 14 human subjects measured inferior vena cava volume with an impedance catheter during normal, quiet respiration. This study noted that extrathoracic inferior vena cava volume rose with expiration while intrathoracic inferior vena cava volume decreased with expiration [20]. "Extrathoracic inferior vena cava" describes the region of the vena cava that lies below the diaphragm, and "intrathoracic inferior vena cava" refers to the region of the inferior vena that lies above the diaphragm. Based on these earlier studies, volume of the abdominal inferior vena cava (i.e., below the diaphragm) should be at a minimum at end inspiration; at end expiration, the volume should be at a maximum.

Even though the breath hold data from the present study was not statistically significant, an evaluation of the trends in the data may offer some additional insight. During control, volume of men's inferior vena cava was 5.2% smaller at end expiration than at end inspiration. During LBNP, the contrast was more substantial with a decrease of 27.4% from end inspiration to end expiration. During LBNP, volume of women's inferior vena cava decreased 2.7% from end inspiration to end expiration. The expected contrast in volume of the inferior vena cava was apparent only in women during control when inferior vena cava volume was 12.5% larger at end expiration than at end inspiration.

The reasons for the inconsistencies within data of the present study as well as between the present study and those of other studies are not clear. The data could have been affected if subjects strained themselves during breath holds. The length of time for every breath hold was constant across all subjects, but the ability to hold one's breath varies from person to person. Some subjects may have also found one breath

hold to be more difficult than the other. Because some subjects may have struggled to maintain the breath holds, the data may have been affected by strain, thereby compromising the comparisons between breath holds.

The inconsistencies could also be a result of tethering of the vessel walls to the surrounding tissue, making it less responsive to breathing than segments measured in other studies. It appears that the other studies measured the effect of respiration on a different part of the inferior vena cava than the segment analyzed in the present study and, therefore, could have different tethering to their surrounding tissues.

The inconsistencies could also be a result of differences in experimental protocols. While the present study isolated end expiration and end inspiration by requiring test subjects to hold their breath, the other studies measured size of the inferior vena cava during normal, quiet respiration. Perhaps response to the transient disturbance of normal breathing differs from response during steady-state breath holds. For example, just as the width of the inferior vena cava partially recovered during the first 60 seconds of steady-state LBNP following LBNP ramp-up, changes to inferior vena cava volume may have also recovered during steady-state breath holds following normal breathing.

Inconsistencies during LBNP in the present study could be a consequence of the orthostatic stress itself. The impact of LBNP upon the inferior vena cava could be so much more significant than the impact of respiration that it effectively masks variations due to breathing. The difference in intrapleural pressure between end expiration and end inspiration is roughly 4 cm H_2O or 2.9 mmHg [6]. Even though LBNP was directly applied to the body below the inferior vena cava (beginning at the iliac crest of the hip), its effect upon the inferior vena cava was both statistically and physiologically significant. The –35 mmHg stress could very likely impact inferior vena cava volume far more than the 2.9 mmHg oscillation of respiration.

While changes to inferior vena cava dimensions due to respiration appear unclear, the observed consistent and sizable volume decrease resulting from LBNP merits a key question: Was the impact of LBNP on vena cava size real, or was it an indication of vessel displacement along the Z-axis (stretching/compression, sliding)? Recall this study's use of a rigid coordinate system, focusing on a fixed 3.6 cm space

rather than on a fixed 3.6 cm length of the inferior vena cava. Consequently, movement by the vessel along the Z-axis was not captured by the images and therefore possibly influenced the accuracy of the data.

On the other hand, if the inferior vena cava slid along the Z-axis during LBNP, it would have slid away from the heart, toward the abdomen. Because the inferior vena cava gets wider as it approaches the heart, we would expect this displacement to be seen as an increase in axial cross-sectional area and in coronal width. Although this certainly may have happened, the vessel's tendency to collapse during LBNP was far more evident than any displacement that might have occurred. Even if the vessel slid along the Z-axis, this movement does not decrease the significance of our observations regarding volume and width of the inferior vena cava. Rather, the possibility of displacement could make the observed changes even more significant physiologically because a wider section closer to the heart during control would have had to slide along the Z-axis and collapse even more than the segment that was visualized during control.

5.2 Inferior Vena Cava Width as a Function of Changes in LBNP

The observed changes in inferior vena cava width at portal entry and at portal exit during all three phases of LBNP (ramp-up, steady-state, and ramp-down) supplement existing knowledge of cardiovascular response to orthostatic stress. Reductions in vena cava width at portal entry and at portal exit suggest that transmural pressure at both measurement sites dropped as a result of LBNP. In order for transmural pressure to decrease, the intravascular pressure at these two measurement sites must have dropped because the body at the measurement sites was outside the LBNP chamber and was therefore at atmospheric pressure during the measurements. Indeed, in another study conducted in our laboratory, central venous pressure was measured during LBNP and revealed that central venous pressure in the thoracic region decreases as LBNP becomes more negative. Figure 5.1 illustrates this relationship between central venous pressure and LBNP.

Venous pooling in the lower extremities is a well-documented result of LBNP, and this response apparently does not extend up to the abdominal inferior vena cava. A static region of the venous circulation must exist somewhere in between the collapsing

inferior vena cava and the distending veins of the lower extremities. Presumably, no change in volume would be observed at this transition point. One possible location for this transition point could be somewhere near the level of the iliac crest since that region marks the boundary between atmospheric pressure and negative pressure.

The inferior vena cava's response to all three phases of LBNP is most likely a result of four factors: 1) the vessel's intrinsic mechanical properties (i.e., its basic material compliance), 2) its physical connections (i.e. tethering and anchoring of the vessel) to surrounding tissues, 3) physiological control of vessel width (e.g., vasodilation/vasoconstriction as a result of neural and/or hormonal mechanisms), and 4) fluid volume regulation by the cardiovascular system in response to the orthostatic stress. Factors 2 and 3 when added to factor 1 produce an "effective compliance". Factor 4 relates to the fact that the segment under examination is in a closed fluid circuit that can absorb or release fluid and therefore change intravascular pressure and fluid volume in response to orthostatic stress and associated neurally mediated responses[21]. The change in intravascular pressure can also contribute to change in transmural pressure, resulting in change to vessel width.

Therefore, in the present study, all four factors could be responsible for observed differences in vena cava response at portal entry and at portal exit: 1) the material compliance of the inferior vena cava at the portal exit could be higher than at portal entry; 2) the effective compliance at the portal exit could be higher than at portal entry because of tissue surrounding, tethering, and anchoring the vessel and/or because of vasoconstriction/vasodilation; 3) a change in the blood pressure gradient could have occurred along the length of the inferior vena cava due to changes of fluid moving into the circulation in response to the onset of LBNP.

For example, the inferior vena cava exhibited a partial recovery during the first minute of steady-state LBNP. Further recovery was not apparent at the next data point fourteen minutes later. An increase in plasma volume in response to the first two minutes of –35 mmHg LBNP has previously been reported and is thought to be a direct result of sympathetically mediated vasoconstriction in response to LBNP [21, 22]. The inferior vena cava completely recovered back to its control widths by the end of LBNP ramp-down. The absence of hysteresis when comparing inferior vena cava width during

control and during recovery suggests that there were no relatively long-term residual changes such as creep or relaxation of the vessel's mechanical properties or sustained vasoconstriction or vasodilation after the exposure to LBNP.

Recall that the vessel's response to LBNP ramp-up was a quadratic equation according to Equations 6 and 7. The partial recovery during steady-state LBNP was a linear equation per Equations 8 and 9. The completion of recovery during LBNP ramp-up was a linear equation documented by equations 10 and 11. Thus, recovery during steady-state LBNP could reflect some combination of the vessel's material compliance with cardiovascular regulation (i.e., vasodilation). Recovery during LBNP ramp-down appears to correspond to the inferior vena cava's effective compliance and perhaps to regulation as well. The inferior vena cava recovered from LBNP ramp-up as much as its material compliance allowed while still subjected to a constant –35 mmHg stress. As the –35 mmHg stress diminished toward zero mmHg during LBNP ramp-down, the vessel continued toward its control widths at both measurement sites in a linear fashion, dependent upon the level of LBNP stress. There appears to be a change to the relative contributions of the inferior vena cava's four response factors as LBNP progressed from ramp-up to steady-state and on to ramp-down. While the vessel returned to its control state, the combination of factors dictating its response during LBNP ramp-up appeared to differ from the combination of factors dictating its response during steady-state LBNP and during LBNP ramp-up.

As vessel width increased at both measurement sites during steady-state LBNP, presumably the intravascular pressure at each site also increased. If the change in intravascular pressure during the first minute of steady-state LBNP (dP/dt) was known, the slopes of equations 7 and 8 (change in width per change in time, dW/dt) could be divided by the equivalent change in intravascular pressure to identify the material compliance at each site. This method for calculating material compliance of the inferior vena cava at each site is represented by Equation 12.

$$\text{Material Compliance} = [dW/dt] * [dP/dt]^{-1} \qquad \text{(Eq. 12)}$$

The inferior vena cava's effective compliance can be calculated by using the relationship between LBNP and central venous pressure illustrated in Figure 5.3. The slopes of equations 10 and 11 (change in width per change in LBNP, dW/dP_{LBNP}) can

be divided by the equivalent change in central venous pressure to identify the effective compliance at each site. This method for calculating effective compliance of the inferior vena cava at each site is represented by Equation 13.

$$\text{Effective Compliance} = [dW/ dP_{LBNP}] * [dP_{CV}/ dP_{LBNP}]^{-1} \quad \text{(Eq. 13)}$$

Assuming that the rate of LBNP ramp-down was linear, the result of Equation 13 should match the slopes of Equations 10 and 11.

While all of the interrelationships amongst the possible mechanisms discussed above could have changed from LBNP ramp-up to steady-state LBNP and on to LBNP ramp-down, the specific relative contributions of each factor to the measured response of the inferior vena cava is beyond the scope of the present study.

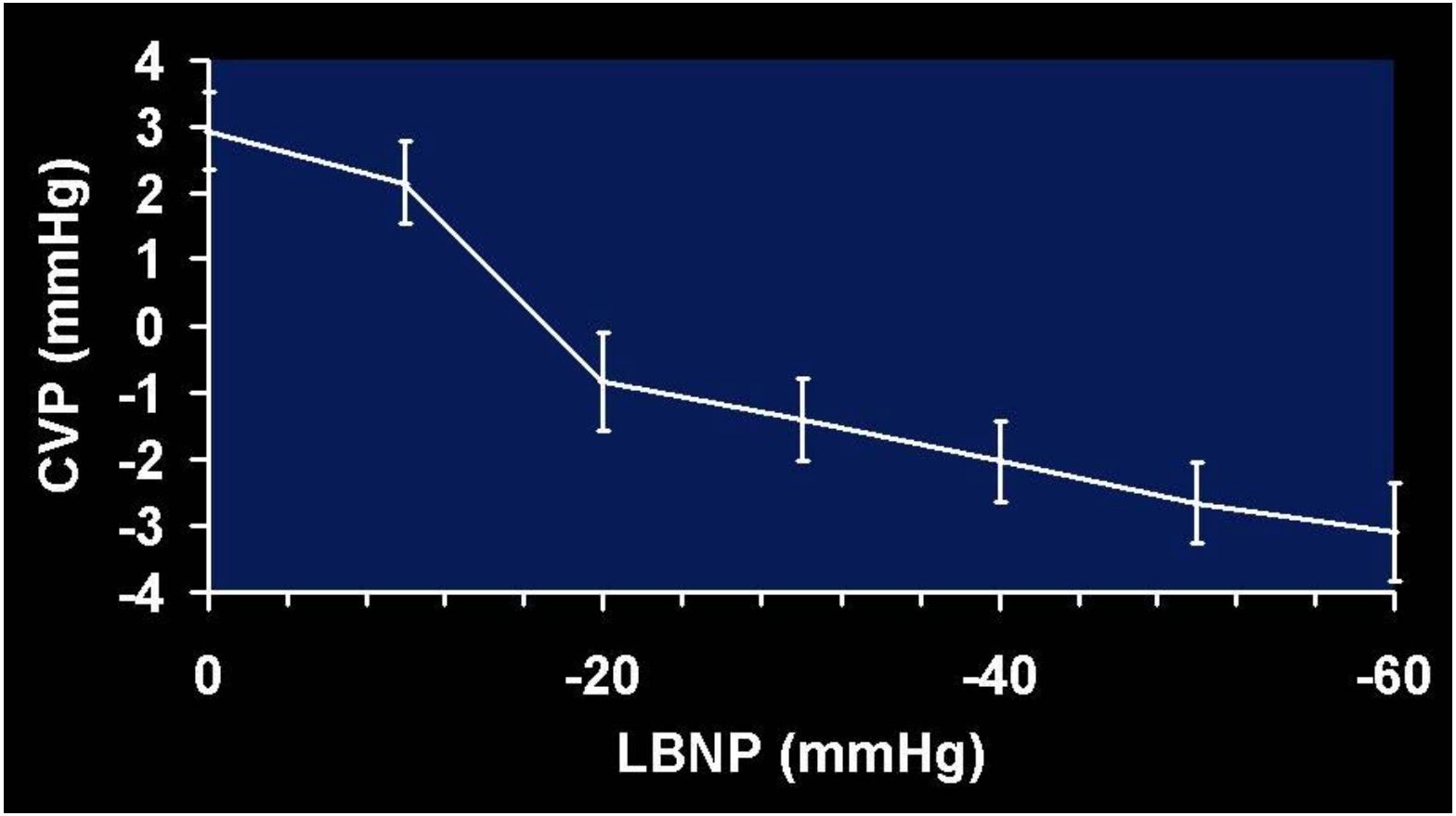

Figure 5.1: Central Venous Pressure vs. Lower Body Negative Pressure

6 Conclusions

Data from this study did not reveal any differences in size of the inferior vena cava between end inspiration and end expiration breath holds in either gender during control and during –35 mmHg LBNP. However, the effects of –35 mmHg lower body negative pressure upon axial cross-sectional area and coronal width of the inferior vena cava were statistically and physiologically important. The present study provided the following major findings:

1) IVC volume for men and women combined decreased 41% due to LBNP ($p < 1.02 \times 10^{-9}$);
2) women's gross IVC volume was 23% smaller than men's during control and LBNP ($p < 0.0005$); however, normalization against body surface area eliminated statistical significance of this difference;
3) the IVC volume change caused by LBNP was not statistically different between genders ($p < 0.696$);
4) respiration had no statistically significant impact on IVC volume ($p < 0.395$);
5) men's IVC width was 64.4% wider at portal exit than at portal entry ($p < 0.0003$);
6) –35 mmHg LBNP induced a decrease in men's vena cava width up to 46% at portal exit and up to 62% at portal entry.

References

[1] Bannister, R. (ed). Autonomic Failure : A Textbook of Clinical Disorders of the Autonomic Nervous System. Oxford: Oxford University Press, 1988.

[2] Meck, J.V., C.J. Reyes, S.A. Perez, A.L. Goldberger, and M.G. Ziegler. "Marked Exacerbation of Orthostatic Intolerance after Long- vs. Short-Duration Spaceflight in Veteran Astronauts." Pscyhosomatic Medicine November-December 2001; 63(6): 865-873.

[3] Garstang, Susan V. "Cardiovascular Concerns in Spinal Cord Injury." eMedicine. August 14, 2001 <http://www.emedicine.com/pmr/topic20.htm>.

[4] Williams, David R. "A Crewed Mission to Mars." National Space Science Data Center. March 20, 2001 <http://nssdc.gsfc.nasa.gov/planetary/mars/marsprof.html>.

[5] Maisel, William H., and William G. Stevenson. "Syncope – Getting to the Heart of the Matter." The New England Journal of Medicine September 2002; 347: 931-933.

[6] Rowell, Loring B. Human Cardiovascular Control. New York: Oxford University Press, 1993.

[7] White, D.D. and L.D. Montgomery. "Pelvic Blood Pooling of Men and Women During Lower Body Negative Pressure." Aviation, Space, and Environmental Medicine June 1996; 67(6): 555-559.

[8] Chang, C.M., Y. Cassuto, D.R. Pendergast, and L.E. Farhi. "Cardiorespiratory Response to Lower Body Negative Pressure." Aviation, Space, and Environmental Medicine July 1994; 65(7): 615-620.

[9] Evans, Joyce M., Fabio M. Leonelli, Michael G. Ziegler, Casey McIntosh, Abhijit Patwardhan, Andrew C. Ertl, Charles S. Kim, Charles F. Knapp. "Epinephrine, Vasodilation and Hematoconcentration in Syncopal, Healthy Men and Women." Autonomic Neuroscience: Basic and Clinical 2001; 93: 79-90.

[10] Beck, L., F. Baisch, F.A. Gaffney, J.C. Buckey, P. Arbeille, F. Patat, A.D. ten Harkel, A. Hillebrecht, H. Schulz, and J.M. Karemaker. "Cardiovascular

Response to Lower Body Negative Pressure Before, During, and After Ten Days Head-Down Tilt Bedrest." Acta Physiologica Scandinavica Supplement 1992; 604: 43-52.

[11] Stewart, Julian M., Marvin S. Medow, Barbara Bassett, and Leslie D. Montgomery. "The Effect of Thoracic Blood Volume on the Valsalva Maneuver." American Journal of Physiology – Heart and Circulatory Physiology August 2004; 287: H798-H804.

[12] Stewart, Julian M. and Leslie D. Montgomery. "Regional Blood Volume and Peripheral Blood Flow in the Postural Tachycardia Syndrome." American Journal of Physiology – Heart and Circulatory Physiology September 2004; 287: 10.1152/ajpheart.01174.2003.

[13] Unterweger, M., J.F. Debatin, D.A. Leung, S. Wildermuth, G.C. McKinnon, G.K. von Schulthess. "Cardiac Volumetry. Comparison of Echoplanar and Conventional Cinemagnetic Resonance Data-Acquisition Strategies." Investigative Radiology November 1994; 29(11): 994-1000.

[14] Westbrook, Catherine and Carolyn Kaut. MRI In Practice, second edition. United Kingdom: Blackwell Science, 1998.

[15] Nishimura, Dwight G. Principles of Magnetic Resonance Imaging. Palo Alto: Stanford University Department of Electrical Engineering, 1996.

[16] Schiebler, M.L., J. Listerud, G. Holland, R. Owen, R. Baum, and H.Y. Kressel. "Magnetic Resonance Angiography of the Pelvis and Lower Extremities. Works in Progress." Investigative Radiology Supplement December 1992; 27(Suppl 2): S90-S96.

[17] McVeigh, Elliot and Ergin Atalar. "Cardiac Tagging With Breath-hold CINE MRI." Magnetic Resonance in Medicine 1992; 28: 318-327.

[18] QuantIm User Manual. Zedec Technologies, Inc. 1995.

[19] Smith, H.J., P. Grottum, and S. Simonsen. "Ultrasonic Assessment of Abdominal Venous Return. I. Effect of Cardiac Action and Respiration on Mean Velocity Pattern, Cross-Sectional Area, and Flow in the Inferior Vena Cava and Portal Vein." Acta Radiologica: Diagnosis (Stockholm) Sep-Oct 1985; 26(5): 581-588.

[20] Ferguson, J.J. 3rd, M.J. Miller, P. Sahagian, J.M. Aroesty, and R.G. McKay. "Effects of Respiration and Vasodilation on Venous Volume in Animals and Man, as Measured with an Impedance Catheter." Catheterization and Cardiovascular Diagnosis January 1989; 16(1): 25-34.

[21] Hinghofer-Szalkay, H., E.M. Konig, G. Sauseng-Felleger, and C. Zambo-Polz. "Biphasic Blood Volume Changes With Lower Body Suction in Humans." The American Physiological Society 1992: H1270-H1275.

[22] Evans, J.M, F.M. Leonelli, M.G. Ziegler, C. McIntosh, A.R. Patwardhan, A.C. Ertl, C.S. Kim, and C.F. Knapp. "Epinephrine, Vasodilation and Hemoconcentration in Syncopal, Healthy Men and Women." Autonomic Neuroscience: Basic & Clinical 2001; 93: 79-90.

Vita

Birth:

White Pine, Michigan 1974

Education:

Bachelor of Science, Electrical Engineering and Computer Science with focus in Bioelectronics from University of California, Berkeley

Professional Positions:

Design Electrical Engineer - General Electric Medical Systems (1999 – 2000)

Senior Technical Operations Engineer - Beckman Coulter (2001 – present)

Scholastic and Professional Honors:

Kentucky Governor's Scholar Finalist

National Merit Scholar Finalist

U.S. President Scholar Semifinalist

2004 Beckman Coulter Circle of Excellence Nominee

Conference Presentations:

"Differences Between Heart Rate Spectral Power From Human Subjects on High and Low Salt Diets." Experimental Biology: Anaheim, CA, 1992.

"Gender Differences in Cardiovascular Response to Lower Body Negative Pressure as Measured through Magnetic Resonance Angiography." V.Pothini, J.Evans, A.Griffin, L.Hilaire, G.Robson, C.Knapp. Biomedical Engineering Society: San Diego, CA 1997.

"Vena Cava Response to Lower Body Negative Pressure as Measured with Magnetic Resonance Imaging." V.Pothini, L.Hilaire, J.Evans, C.Knapp. Experimental Biology: San Francisco, CA, 1998.